ISSN 1674-1056
http://cpb.iphy.ac.cn
http://iopscience.iop.org/cpb
中国物理 B
Chinese Physics
中国物理 Chinese Physics B

# Optical phonon behavior and magnetism of columbite $Zn_{0.8}Co_{0.2}Nb_2O_6$

Liang Li(李亮)[1], Xiaohan Wang(王晓晗)[1], Ying Liu(刘莹)[1,2], Fangfei Li(李芳菲)[1], Qiang Zhou(周强)[1], Tian Cui(崔田)[1]
**Citation:**Chin. Phys. B . 2019, 28(12): 128104 . **doi:** 10.1088/1674-1056/ab5438
Journal homepage: http://cpb.iphy.ac.cn; http://iopscience.iop.org/cpb

**What follows is a list of articles you may be interested in**

---

## Synthesis and surface plasmon resonance of Au-ZnO Janus nanostructures

Jun Zhou(周俊), Jian-Shuo Zhang(张建烁), Guo-Yu Xian(冼国裕), Qi Qi(齐琦), Shang-Zhi Gu(顾尚志), Cheng-Min Shen(申承民), Zhao-Hua Cheng(成昭华), Sheng-Tai He(何声太), Hai-Tao Yang(杨海涛)
Chin. Phys. B . 2019, 28(8): 083301 . **doi:** 10.1088/1674-1056/28/8/083301

## Effect of metal fluorides on chromium ions doped bismuth borate glasses for optical applications

L Haritha, K Chandra Sekhar, R Nagaraju, G Ramadevudu, Vasanth G Sathe, Md. Shareefuddin
Chin. Phys. B . 2019, 28(3): 038101 . **doi:** 10.1088/1674-1056/28/3/038101

## Measurement of transient Raman spectrum on gas-gun loading platform and its application in liquid silane

Yi-Gao Wang(汪贻高), Fu-Sheng Liu(刘福生), Qi-Jun Liu(刘其军), Wen-Peng Wang(王文鹏), Ming-Jian Zhang(张明建), Feng Xi(习锋), Ling-Cang Cai(蔡灵仓), Ning-Chao Zhang(张宁超)
Chin. Phys. B . 2017, 26(10): 103301 . **doi:** 10.1088/1674-1056/26/10/103301

## Synthesis and application of $TiO_2$ single-crystal nanorod arrays grown by multicycle hydrothermal for dye-sensitized solar cells

Zhu Jian-Jing, Zhao Yu-Long, Zhu Lei, Gu Xiu-Quan, Qiang Ying-Huai
Chin. Phys. B . 2014, 23(4): 048104 . **doi:** 10.1088/1674-1056/23/4/048104

## Interface evolution of a particle in a supersaturated solution affected by a far-field uniform flow

Chen Ming-Wen, Wang Zi-Dong
Chin. Phys. B . 2013, 22(9): 098104 . **doi:** 10.1088/1674-1056/22/9/098104

---

RAPID COMMUNICATION

# Optical phonon behavior and magnetism of columbite $Zn_{0.8}Co_{0.2}Nb_2O_6$*

Liang Li(李亮)[1], Xiaohan Wang(王晓晗)[1], Ying Liu(刘莹)[1,2], Fangfei Li(李芳菲)[1], Qiang Zhou(周强)[1,†], and Tian Cui(崔田)[1]

[1] *State Key Laboratory of Superhard Materials, College of physics, Jilin University, Changchun* 130000, *China*
[2] *Changchun Institute of Technology, Changchun* 130012, *China*

(Received 8 October 2019; revised manuscript received 1 November 2019; published online 29 November 2019)

Columbite $Zn_{0.8}Co_{0.2}Nb_2O_6$ crystals were grown by optical floating zone methods. The x-ray diffraction (XRD) was used to check the structure information of the grown $Zn_{0.8}Co_{0.2}Nb_2O_6$ crystal. The room temperature and temperature-dependent Raman spectra were tested to investigate the optical phonon behaviors of columbite $Zn_{0.8}Co_{0.2}Nb_2O_6$, which exhibited a temperature stable property. The magnetics properties of $Zn_{0.8}Co_{0.2}Nb_2O_6$, measured by a physical property measurement system (PPMS), were also presented in this work.

**Keywords:** columbite $Zn_{0.8}Co_{0.2}Nb_2O_6$, optical floating zone methods, Raman spectra, magnetics properties

**PACS:** 81.10.Aj, 33.20.Fb, 61.05.Cp, 07.55.Jg **DOI:** 10.1088/1674-1056/ab5438

## 1. Introduction

The columbite structure $ZnNb_2O_6$ is a wide-bandgap semiconductor (3.84 eV)[1] and a typical good performance microwave dielectric material.[2,3] In the lattice, $Zn^{2+}$ and $Nb^{5+}$ are encircled by six oxygen atoms, thereby forming $ZnO_6$ and $NbO_6$ octahedrons. The $ZnO_6$ and $NbO_6$ octahedrons share oxygen atoms through edge, and an independent zigzag chain is formed along the *c*-axis. Along the *a*-axis direction, $ZnO_6$ and $NbO_6$ octahedrons are connected by corner-sharing oxygen atoms, forming $ZnO_6$–$NbO_6$–$NbO_6$–$ZnO_6$ arrangement. This arrangement generally appears as a layered structure of ZnNbNbZnNbNb.[4,5] Significantly, this arrangement allows the columbite structure materials to exhibit excellent optical, magnetic, and electric properties.[2,6–8]

Studies on diluted magnetic semiconductors have mainly focused on the doping of transition metals into an oxide semiconductor with a wide bandgap.[9–11] For the oxide based dilute magnetic semiconductor, the doping of transition metal ions is an important method to control the magnetic performance and may significantly influence the electrical conductivity, dielectric properties, and other physical performances.[12–14] The $ZnNb_2O_6$ doped with transition metal ions may present different performances and thus should be investigated. However, there are not very many studies concerning the magnetic performance of the $ZnNb_2O_6$ compound doped with cobalt ions.

Meanwhile, the single crystal samples exhibit integrated structures and explicit growth direction and are free of defects and impurities.[15] They are the most appropriate samples for understanding the intrinsic characteristics of the materials. Thus far, no study on the single-crystal growth of cobalt-doped $ZnNb_2O_6$ has been reported besides our previous work.[16] Therefore, the growth of $Zn_{0.8}Co_{0.2}Nb_2O_6$ single crystals must be of great value. Moreover, the intrinsic magnetism of the materials should be understood. In this work, $Zn_{0.8}Co_{0.2}Nb_2O_6$ single crystals were grown successfully via optical floating zone methods for the first time. The optical and magnetic properties were characterized through a series of experiments, aiming at the optical and magnetic applications.

## 2. Experiment procedure

The powder was prepared by the traditional solid-state reaction technique to mix stoichiometry amount ZnO, $Nb_2O_5$, and CoO from Alfa Aesar company with 4N purity in air at 1300 °C for 20 h with intermediate grindings. The nominal content $Zn_{0.8}Co_{0.2}Nb_2O_6$ single crystals were grown by the Crystal Systems Inc. infrared-heating floating-zone furnace (model: FZ-T-10000-H-VP-VI) in the air atmosphere.

The x-ray diffraction (XRD) spectra were acquired by an x-ray diffractometer from Rigaku (model: RU-200b) with a Cu $K\alpha$ radiation source. A Rigaku Micro Max-007HF two-dimensional x-ray diffractometer ($XRD^2$) was also employed to tested the growth directions of the crystals. The Raman spectra were recorded by a Jobin-Yvon LABRAM-HR 800 high resolution Raman spectroscope with 514.5 nm exciting laser from Spectrum Physics (model: Stable 2017). The Quantum Design physical property measurement system (model:

*Project supported by the National Key Research and Development Program of China (Grant No. 2017YFA0403704), the National Natural Science Foundation of China (Grant Nos. 11304113, 11474127, and 11574112), and the Fundamental Research Funds for the Central Universities of China.

†Corresponding author. E-mail: zhouqiang@jlu.edu.cn

© 2019 Chinese Physical Society and IOP Publishing Ltd 

PPMS-16) was used to obtain the magnetization $M$ versus magnetic field $H$ and magnetic susceptibility $\chi$ versus temperature $T$ curves.

## 3. Results and discussion

The grown $Zn_{0.8}Co_{0.2}Nb_2O_6$ single crystal pieces were ground into powder in a mortar. Then, the XRD spectra of the $Zn_{0.8}Co_{0.2}Nb_2O_6$ powder samples were obtained through XRD tests. The XRD spectrum of the powder sample was refined via Rietveld method by using MAUD software with Sig. $= 1.41$. Figure 1(a) shows the refined XRD spectrum. The $Zn_{0.8}Co_{0.2}Nb_2O_6$ has the columbite structure and belongs to the *Pbcn* space group. The lattice parameters of $Zn_{0.8}Co_{0.2}Nb_2O_6$ are $a = 14.190$ Å, $b = 5.724$ Å, $c = 5.037$ Å, which are slightly smaller than those of the pure $ZnNb_2O_6$ samples ($a = 14.208$ Å, $b = 5.726$ Å, $c = 5.04$ Å). The radius of $Co^{2+}$ is 0.650 Å at low spin state and 0.745 Å at high spin state. In $Zn_{0.8}Co_{0.2}Nb_2O_6$, the low and high spin states should co-exist at the same time. Then the average radius of $Co^{2+}$ is slightly smaller than that of $Zn^{2+}$ (0.740 Å). So $Co^{2+}$ can replace $Zn^{2+}$ without causing abundant mismatching of the crystal lattice. No impurity peak is observed in the entire XRD spectrum, indicating that the growing crystal is columbite structure $Zn_{0.8}Co_{0.2}Nb_2O_6$ without impurity. Moreover, the crystal sample matches well with the original columbite structure and the dopant reduces the crystal lattice slightly. The XRD$^2$ result, as shown in Fig. 1(b), was tested on the wafer cut vertical the growth direction of the $Zn_{0.8}Co_{0.2}Nb_2O_6$ crystal. There is only one peak located at 64.2°. It indicates that the crystal grows along the ⟨191⟩ direction.

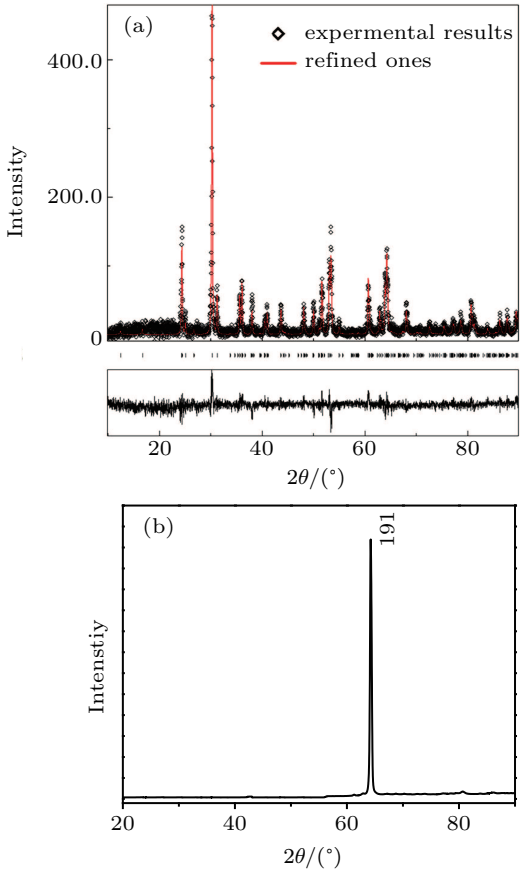



**Fig. 1.** (a) Rietveld method refined XRD spectrum of $Zn_{0.8}Co_{0.2}Nb_2O_6$ powder samples, and (b) XRD$^2$ spectrum of the crystal wafer.

Room temperature Raman spectrum of $Zn_{0.8}Co_{0.2}Nb_2O_6$ crystal has been measured. The result is shown in Fig. 2. It can be found that all Raman peaks in the spectrum can be indexed to columbite structure $ZnNb_2O_6$.[17] The peak position shifts to the lower wavenumber direction. The strongest Raman peak, corresponding to the symmetrical stretching vibration of Nb–O bond, is fitted by a Gaussian function. Its peak location is 890 cm$^{-1}$ and its full width of half-maximum (FWHM) is 15 cm$^{-1}$. The peak center and the FWHM of the strongest symmetrical stretching vibration of Nb–O bond in the undoped columbite structure $ZnNb_2O_6$ are 894 cm$^{-1}$ and 7 cm$^{-1}$, respectively. The changes are obviously. When the $Co^{2+}$ ions are doped into the columbite structure $ZnNb_2O_6$, the lattice parameters change as shown in the XRD results and the microscope structure is also affected by the $Co^{2+}$. The bond energy, electronegativity, and the uniforms of the bonds become lower.

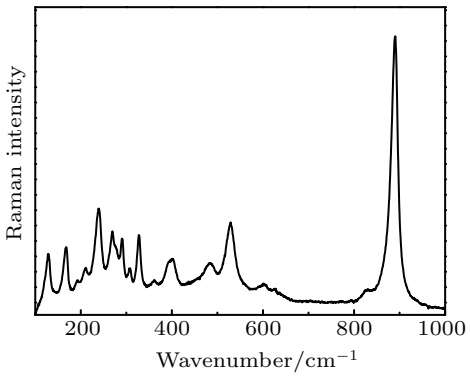



**Fig. 2.** Room temperature Raman spectrum.

The temperature-dependent Raman tests of the as-grown $Zn_{0.8}Co_{0.2}Nb_2O_6$ crystal were conducted to understand the optical phonon behaviors of $Zn_{0.8}Co_{0.2}Nb_2O_6$ at different temperatures. The Raman spectra were recorded at every 40 °C from −180 °C to 500 °C. Thus, 18 temperature-dependent Raman spectra were recorded, as shown in Fig. 3(a). A total of 19 recognizable Raman bands could be observed at −180 °C and all of the Raman bands can be indexed well with those of the undoped columbite $ZnNb_2O_6$ samples. With the increase in temperature, the Raman peak moves toward the low wave number, accompanied with a continuous linewidth growth and gradual intensity decrease. As a result, weak Raman peaks disappear or overlap. Only 10 Raman peaks can be distinguished well at 500 °C. And no new Raman peak was observed throughout the process. In the whole temperature range, we fit four typical Raman bonds, the stretching

vibration of terminal bond at 888 $cm^{-1}$, the stretching vibration of Nb–O bridged bond at 527 $cm^{-1}$, the bending vibration of O–Nb–O bond at 280 $cm^{-1}$, and the stretching vibration of Nb–Nb bond between $NbO_6$ octahedron links at 127 $cm^{-1}$, with Gaussian, and give the curves of Raman wavenumber and FWHM varying with temperature in Figs. 3(b) and 3(c), respectively. In the whole range, all of the temperature dependent Raman wavenumber and three FWHW curves can be fitted linearly. The bond at 127 $cm^{-1}$ shows an abnormal phenomenon at low temperature (from −180 °C to −60 °C). The Nb–Nb bond is a weak interaction and the uniform of the Nb–Nb bond is improved from −180 °C to −60 °C. Hence, the optical phonon modes of $Zn_{0.8}Co_{0.2}Nb_2O_6$ are stable in this temperature interval. This result reflects the good thermostability of $Zn_{0.8}Co_{0.2}Nb_2O_6$ in this temperature range.

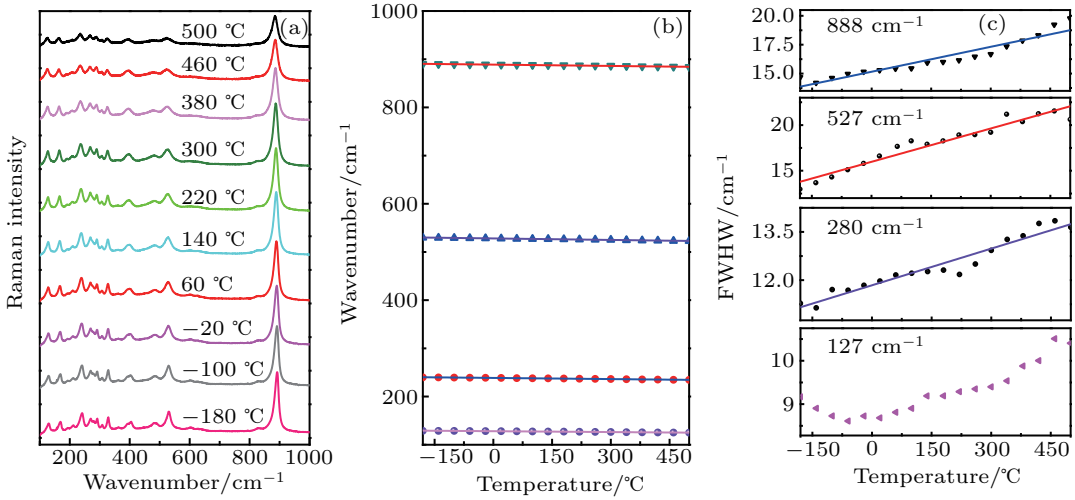



**Fig. 3.** (a) Temperature-dependent Raman spectra of $Zn_{0.8}Co_{0.2}Nb_2O_6$; the curves of Raman wavenumber (b) and FWHM (c) varying with temperature.

The FC curves of the samples in the temperature range of 300–3 K under the external field of 500 Oe were measured, thereby obtaining the relation between the magnetic susceptibility and temperature (Fig. 4). The FC curves increase with the reduction of temperature. No splitting occurs at the lowest temperature (3 K). This result conforms to the observation results of $CoNb_2O_6$ in Refs. [18]–[20]. While, as the magnetic susceptibility is relatively smooth in the high-temperature region, some parts must be unrelated with temperature. Hence, the magnetism is composed of two parts, namely, the Curie–Weiss paramagnetism related with temperature and the Pauli paramagnetism unrelated with temperature[21]

$$\chi(T) = \frac{C}{T - T_0} + \chi_{\rm pp},$$

where $C$ is the Curie–Weiss constant and $T_0$ is the Curie–Weiss temperature. Figure 3 shows the variation law of reciprocals of the Curie–Weiss magnetic susceptibility with temperature, in which $T_0$ is approximately 1 K. This result demonstrates that no antiferromagnetic interaction occurs in the samples.[21,22] The $C$ is fitted to be 0.82 emuK/Oe·mol, and the effective magnetic moment is calculated to be 1.85 $\mu_B$/Co, which is higher than the low spin state value (1 $\mu_B$) and lower than the high spin state one (3 $\mu_B$). Thus, the low and high spin states are coexisting in $Zn_{0.8}Co_{0.2}Nb_2O_6$, which agrees well with the XRD result.

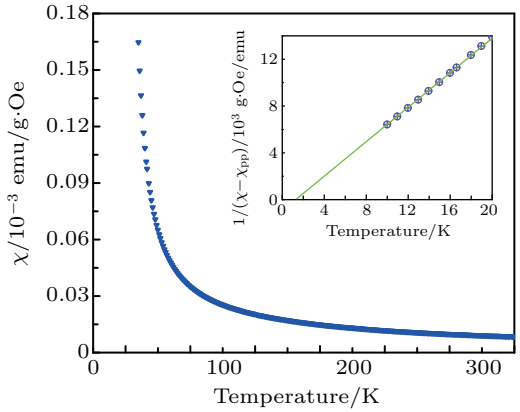



**Fig. 4.** Temperature dependent magnetic susceptibility of $Zn_{0.8}Co_{0.2}Nb_2O_6$ sample from 300 K to 3 K.

The $M$–$H$ curve of the $Zn_{0.8}Co_{0.2}Nb_2O_6$ powder was also tested by using the PPMS. The temperatures were set at 300 K, 20 K, and 5 K as shown in Fig. 5. The externally applied magnetic field ranged from −9 T to 9 T. At 300 K and 20 K, $Zn_{0.8}Co_{0.2}Nb_2O_6$ exhibits paramagnetism. When the temperature is 5 K, a weak magnetic hysteresis occurs, indicating the existence of ferromagnetism. It shows a similar behave with our previous work.[16] As illustrated in Fig. 5, the area surrounding the 5 K zero field is amplified, and the coercivity is approximately 0.0018 T, which is lower than the $Zn_{0.9}Co_{0.1}Nb_2O_6$ ones.[16] The ferromagnetism becomes saturated when the external field is increased to 9 T. The columbite $ANb_2O_6$ can be viewed as a layered struc-

ture of A–Nb–Nb–A–Nb–Nb. The $Zn^{2+}$ and $Co^{2+}$ ions occupy the A site randomly in $Zn_{0.8}Co_{0.2}Nb_2O_6$. The doped $ZnNb_2O_6$, compared with $CoNb_2O_6$, does not destroy the 1D ferromagnetic chain of the original system, but it influences the antiferromagnetism of the 2D isosceles triangular lattices. The $CoNb_2O_6$ is reported to be antiferromagnetism. When nonmagnetic ion $Mg^{2+}$ is doped into $CoNb_2O_6$ to replace $Co^{2+}$, the original antiferromagnetism disappears. The $Zn_{0.8}Co_{0.2}Nb_2O_6$ can also be viewed as $Zn^{2+}$ doped into $CoNb_2O_6$. In $Zn_{0.8}Co_{0.2}Nb_2O_6$, no antiferromagnetism is observed, which conforms to the previously reported results of $Mg^{2+}$ doped $CoNb_2O_6$.[23,24]

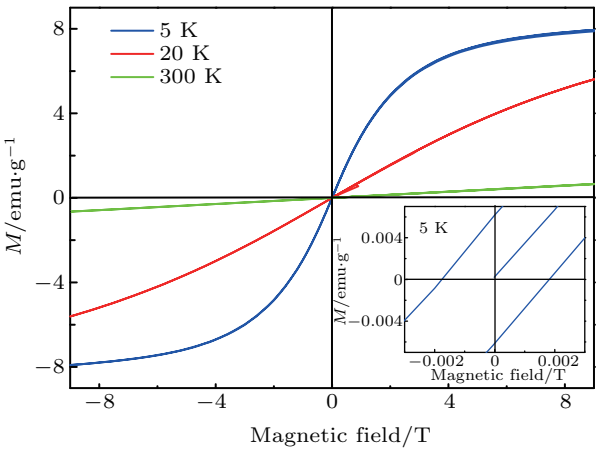



**Fig. 5.** The *M*–*H* curve of $Zn_{0.8}Co_{0.2}Nb_2O_6$.

## 4. Conclusion

The columbite $Zn_{0.8}Co_{0.2}Nb_2O_6$ crystals were grown via infrared heating optical floating zone methods. The XRD results show that the $Zn_{0.8}Co_{0.2}Nb_2O_6$ crystals grow along ⟨191⟩ direction and have the columbite structure with *Pbcn* space group, and the lattices parameters are $a = 14.190$ Å, $b = 5.724$ Å, $c = 5.037$ Å. The room temperature Raman spectrum shows the bond energy and the uniforms of the bonds become lower when $Co^{2+}$ ions are doped. The temperature dependent Raman spectra indicated that $Zn_{0.8}Co_{0.2}Nb_2O_6$ is stable in the whole temperature range. The Curie–Weiss temperature is 1 K and when the temperature is down to 5 K, $Zn_{0.8}Co_{0.2}Nb_2O_6$ exhibits a weak ferromagnetism.

## References

[1] Xu D, Gu Y, Li L, Shen H, Yang H, Zhou Q, Shi Z, Yuan H and Cui T 2014 *J. Phys. Chem. Solids* **75** 1361
[2] Coldea R, Tennant D, Wheeler E, Wawrzynska E, Prabhakaran D, Telling M, Habicht K, Smeibidl P and Kiefer K 2010 *Science* **327** 177
[3] Pullar R C 2009 *J. Am. Ceram. Soc.* **92** 563
[4] Zhao D, Ma F X, Zhang R J, Li F F, Zhang L, Yang J, Fan Y C and Xin X 2016 *Cryst. Eng. Comm.* **18** 2929
[5] Xu D, Yang H, Li L, Zhou Q, Yuan H and Cui T 2014 *Cryst. Res. Technol.* **49** 502
[6] Ekmekci M K, Ilhan M, Guleryuz L F and Mergen A 2017 *Optik* **128** 26
[7] Morris C M, Aguilar R V, Ghosh A, Koohpayeh S M, Krizan J, Cava R J, Tchernyshyov O, McQueen T M and Armitage N P 2014 *Phys. Rev. Lett.* **112** 137403
[8] Kinross A W, Fu M, Munsie T J, Dabkowska H A, Luke G M, Sachdev S and Imai T 2014 *Phys. Rev. X* **4** 031008
[9] Mustafa L, Anjum S, Waseem S, Khurshid H and Javed S 2015 *Mater. Today: Proc.* **2** 5638
[10] Ungar F, Cygorek M and Axt V M 2019 *Phys. Rev. B* **99** 195309
[11] Gao X, Wang Q, Sun G, Li C X and Hu L 2016 *Chin. Phys. B* **25** 26801
[12] Zhou Y, Qiu Z, Lü M, Ma Q, Zhang A, Zhou G, Zhang H and Yang Z 2007 *J. Phys. Chem. C* **111** 10190
[13] Tian C, Huang X L, Huang Y P, Li X, Zhou D, Wang X and Cui T 2019 *Chin. Phys. Lett.* **36** 106101
[14] Yu X, Cui H, Zhu M, Xia Z and Sai Q 2019 *Chin. Phys. B* **28** 77801
[15] Zheng L, Wang G F, Qiu M L, Chu Y J, Xu M and Yin P 2017 *Chin. Phys. Lett.* **34** 087801
[16] Liu Y, Xu D, Yu H, Cui T and Li L 2019 *Mod. Phys. Lett. B* **33** 1950274
[17] Xu D, Liu Y, Zhou Q, Cui T, Yuan H, Wang W, Shi Z and Li L 2015 *J. Alloys Compd.* **618** 694
[18] Chang C E and Wilcox W R 1976 *Int. J. Heat Mass Transfer* **19** 355
[19] Nakajima T, Mitsuda S, Okano H, Inomoto Y, Kobayashi S, Prokes K, Gerischer S and Smeibidl P 2014 *J. Phys. Soc. Jap.* **83** 094723
[20] Sarvezuk P W C, Kinast E J, Colin C V, Gusmão M A, da Cunha J B M and Isnard O 2011 *J. Appl. Phys.* **109** 07E160
[21] Hosseinpour P M, Panaitescu E, Heiman D, Menon L and Lewis L H 2013 *J. Mater. Res.* **28** 1304
[22] Che X, Li L and Li G 2016 *Appl. Phys. Lett.* **108** 143102
[23] Nakajima T, Mitsuda S, Inomoto Y, Prokes K, Sikolenko V, Gerischer S and Kobayashi S 2014 *Phys. Rev. B* **90** 064431
[24] Yu T, Yu X, Yang E, Sun C, Zhang X and Lei M 2019 *Chin. Phys. B* **28** 067501